Development of novel and low-cost readout electronics for large FOV gamma camera detector

Aram Radnia
Tehran University of Medical Sciences
Amirhossein Alikhani
Tehran University of Medical Sciences
Behnoosh Teimourian
Tehran University of Medical Sciences
Mahyar Youser Nejad
Tehran University of Medical Sciences
Mohammad Hossein Farahani
Tehran University of Medical Sciences
Fakhereh Pashaei
Radiation Sciences Research Center (RSRC), Aja University of Medical Sciences, Tehran
Arman Rahmim
Departments of Radiology and Physics & Astronomy, University of British Columbia, Vancouver, BC
Mohammad Reza Ay (mohammadreza_ay@tums.ac.ir)
Tehran University of Medical Sciences https://orcid.org/0000-0002-5383-4418

Research Article

Keywords: gamma camera, square PMT, readout electronics, NEMA NU1

Posted Date: March 24th, 2023

DOI: https://doi.org/10.21203/rs.3.rs-2712772/v1

Abstract

Objective: Gamma cameras based on scintillation crystals play a crucial role in nuclear medicine. We designed a readout method for a large field-of-view (FOV) gamma detector, reducing N × M analog signals of photomultiplier tubes (PMTs) to N + M analog sums of each row and column, thus improving complexity and cost considerations while preserving image quality.

Methods: In this study, we developed a gamma detector consisting of 48 square PMTs using novel readout electronics, reducing 6 × 8 to 6 + 8 analog signals. All 14 analog signals were converted to digital signals using AD9257 high-speed analog to digital converters (ADC) driven by the SPARTAN-6 family of field-programmable gate arrays (FPGA) in order to calculate the signal integrals. The positioning algorithm was based on the digital correlated signal enhancement (CSE) algorithm, which was implemented in the acquisition software. The performance characteristics of the developed gamma camera were measured using the NEMA NU1 standard.

Results: The measured energy resolution in the developed detector was 8.7%, intrinsic spatial resolution was 3.9 mm, uniformity was within 0.6%, and linearity was within 0.1%.

Conclusions: The performance evaluation demonstrated that the developed detector has proper specifications for imaging purposes.

I. Introduction

Given the extensive use of gamma cameras as a medical diagnostic instrument for the detection of radiopharmaceuticals administered to the patient [1-3], significant research has been performed to improve the performance of gamma cameras [4]. In a gamma camera, first the gamma rays emitted from the patient's body are collimated using a parallel-hole collimator, subsequently interacting in a monolithic scintillation crystal (commonly used NaI(Tl)). The produced light is converted to a signal by an array of large area PMTs[1] located on the opposite side of the crystal. The PMT output pulses are fed into readout electronics to extract the information on both the absorbed energy and the position of the interaction within the crystal [5]. The information is then used to create a 2D distribution map of a radiotracer material administered to the patient. The selected radiotracer is usually a short-lived 99mTc compound [6]. The function of the different organs can be evaluated using the radio-isotope distribution [7, 8].

An optimized camera with high uniformity and linearity and good spatial resolution enables improved visual quality and quantitative accuracy from the obtained images [9]. The quality of the images is determined by different parameters, such as the scintillation crystal, PMT, light guide, readout electronics, positioning algorithm, calibration algorithms, and so on [10-18]. Multiple positioning algorithms have been developed since 1958 to estimate 2-D coordinates of the interaction point position in the gamma camera [1]. Anger logic, based on the center of gravity algorithm, is a well-known method but suffers from poor spatial resolution and strong FOV compression [14]. Different algorithms have been introduced to

improve spatial resolution in gamma cameras [19-22]. Because we used square PMTs in our developed detector, the CSE method was chosen as the positioning method. The digital CSE positioning algorithm has the best performance with square PMT-based gamma cameras [19, 21]. In this algorithm, the rows and the columns of the PMT signals are summed, and subsequently, CSE processes two 1D[2] outputs to achieve a 2D[3] position (x and y) for each event.

Today, gamma camera read-out circuits benefit from full digital methods of processing and analyzing the PMT signal due to gaining higher energy and spatial resolution. In large area detectors, which have high quantity PMTs, full digital methods increase the complexity of read-out circuits, for example, requiring a high number of fast ADCs as well as fast current amplifiers, more professional processor, more complex circuit design, and so forth, resulting in a more expensive acquisition board. By introducing a combination of digital and analog read-out electronics for systems with PMT, the complexity and the cost can be decreased. The majority of gamma cameras commonly use an array of N × M of PMT, each one producing a separate signal. To date, many techniques have been developed to multiplex these individual signals [23]. In this study, we introduce novel readout electronics which reduce N × M analog signals into an N + M analog sum of each row and column. This method reduces analog and digital complexities enabling improved cost design. In what follows, we elaborate on our methods and evaluate the performance of the developed gamma camera.

[1] photomultiplier tubes
[2] one-dimensional
[3] two-dimensional

Ii. Materials And Methods

A. Gamma Camera

Our developed gamma camera utilizes large square PMTs (R6237, Hamamatsu, Japan) and includes an NaI (Tl) crystal with an area of 58´42 cm^2 with a thickness of 9.5 mm attached to an 18-mm thick glass light guide followed by an arrangement of 6´8 square PMTs measuring 76´76 mm^2 in area. A silicon-based compound is used as an optical adhesive to improve the optical coupling between the crystal and the PMTs.

B. Readout Electronics

The large area gamma camera on which this readout method is implemented has 48 large square PMT arranged in a 6´8 matrix array. First, the generated signals of the PMTs were amplified with a series of 48 fast current-feedback amplifiers, and the current signals of PMTs were converted to voltage signals. The amplifier circuit is an amplifier that uses a capacitor in feedback, “a charge sensitive amplifier.” By changing the value of the feedback capacitor in the amplifier circuit, the length of the PMT voltage

signals can be adjusted. To achieve the best quality of signal vs. prevent signal overlap, the length of the signal is set to 1 μsec.

Subsequently, a circuit has been designed to sum up the PMT's signals by rows and columns in an analog. This circuit is a resistor network which contains the same value of resistances. A schematic of this circuit is shown for the row and column in Figure 1. By utilizing analog summation, six signals presenting the sum of row PMTs and eight signals presenting the sum of column PMTs, or 14 signals in total, will be generated instead of 48 signals that represent each of the PMTs in the traditional full digital methods.

All amplification and summation circuits are in the pizza board and its daughter boards inside the detector (Figure 2).

Next, these voltage signals are transformed into differential signals to enhance SNR in conveying these signals to the ADC[4] to be sampled into the digital signals. The ADC utilized in the acquisition board is AD9257 (Analog Devices, U.S.A.), which has an 8-channel input, up to 65 MHz sample rate, 14 bits sampling resolution, and serial output format. The sampling rate of ADCs is set at 20 million samples per second to ensure the quality of sampling and meet the Nyquist frequency. Since the output channels of the ADCs operate in serial mode and transmit data at the rising edge as well as the falling edge of the clock, the frequency of transmitting data from ADC output channels is 140 MHz. As such, it is crucial that the length of all paths from ADC output channels (every 14 of them) to the FPGA[5] chip be the same to ensure the concurrency of the digital signals. The FPGA, which utilized in the signal acquisition board, is XC6SLX100 of the SPARTAN-6 family (Xilinx, U.S.A.). All ADCs and FPGA are in the ACQ board (Figure 3).

The DC value of the digital row/column signals is not constant; rather, it continuously changes at a slow pace. Additionally, some fluctuations and disturbances can be seen in these signals. Subsequently, a pulse DC-rejection module was designed on the FPGA to be immune to sudden and significant changes in the signal value and follow the DC value changes correctly over time. After the DC-rejection module, to measure the value of the row/column AC signals, the threshold pulse integration technique was used to calculate the pulse area of these signals. The obtained integrations were then transmitted to the acquisition computer software for positioning through the UDP Ethernet protocol via the W5300 (WIZnet) chip, and the module that provided this transmission was implemented on the FPGA. The software was written on the Python platform to perform linearity, energy, and uniformity calibrations and to quantitatively evaluate planar images.

C. Positioning

The positioning algorithm utilized to determine the position of the hit gamma-ray into the gamma camera's surface was based on the digital CSE algorithm, because in gamma cameras equipped with large square PMTs, other positioning algorithms such as the Anger algorithm require more sophisticated correction techniques. The digital CSE algorithm requires column and row summation of PMT signals;

this algorithm performs two identical processes to determine the position of each event in 1D, and then combines the results of these two processes to produce a 2D (x and y) position of this event. This algorithm is implemented on the acquisition software on a computer. It processes the x position of each event by getting eight summed-up column signals and obtains the y position of the events by getting six summed-up row signals. All of the input values are summed up and stored as energy values.

D. Calibration

The first step is to adjust the PMTs gain. Then we need to have 2D linearity calibration data acquired with a well-collimated beam of gamma rays normal to the face. Two lead masks with parallel vertical and horizontal slits 1 mm in width and spaced 10 mm from the adjacent ones were used for X and Y linearity calibrations.

The next step was uniformity and energy calibration, and for this purpose we used a Tc-99m point source placed far from the detector face. A minimum of 10 k counts for each central pixel must be collected. These calibration methods have been described in our previous works [19].

[4] analog-to-digital converter
[5] field-programmable gate array

Iii. Results

The performance characteristics of the developed gamma camera were measured using the NEMA NU1 standard [24]. For this purpose, energy resolution, spatial linearity, spatial resolution, and uniformity were measured. In the developed detector, the UFOV[6] is 54×38 cm^2, and the CFOV[7] is 46.7×32.9 cm^2.

The energy spectrum was measured based on NEMA standards. The FWHM[8] energy was 13% before calibration and 8.7% after calibration. Figure 4 shows the energy spectrum for Tc-99m at 140keV after energy calibration.

The uniformity of the detector was measured by placing a point source far from its face. Figure 5 shows the flood-field image before and after uniformity calibration. Intrinsic flood-field uniformity was measured according to the NEMA NU1 standard protocol [24]. Results are shown in Table 1.

Table 1. Intrinsic flood field uniformity

INTRINSIC FLOOD FIELD UNIFORMITY	Value
Differential CFOV (%)	0.4
Differential UFOV (%)	0.4
Integral CFOV (%)	0.4
Integral UFOV (%)	0.6

Figure 6 shows the slit mask lead images after calibrations. The intrinsic differential linearity was measured as the SD[9] of peak locations in slit images. The intrinsic absolute linearity was measured as the maximum displacement of peaks in comparison with parallel lines spaced 10 mm apart fitted to the image. The results regarding intrinsic spatial linearity are available in Table 2. To measure intrinsic spatial resolution (without collimator), an image of 1-mm wide slits spaced 10 mm from the adjacent ones was used. The FWHM and FWTM[10] was calculated using the extracted LSF[11] of each line as spatial resolution. The intrinsic spatial resolution results are reported in Table 3.

Table 2. Intrinsic values of spatial linearity

INTRINSIC SPATIAL LINEARITY		Value
(Horizontal)	**Differential CFOV (mm)**	0.04
	Differential UFOV (mm)	0.04
	Absolute CFOV (mm)	0.04
	Absolute UFOV (mm)	0.04
(Vertical)	**Differential CFOV (mm)**	0.04
	Differential UFOV (mm)	0.04
	Absolute CFOV (mm)	0.1
	Absolute UFOV (mm)	0.1

Table 3. Intrinsic values of spatial resolution

INTRINSIC SPATIAL RESOLUTION		Value
(Horizontal)	FWHM CFOV (mm)	3.9
	FWHM UFOV (mm)	3.9
	FWTM CFOV (mm)	6.9
	FWTM UFOV (mm)	7.0
(Vertical)	FWHM CFOV (mm)	3.7
	FWHM UFOV (mm)	3.7
	FWTM CFOV (mm)	6.8
	FWTM UFOV (mm)	6.8

[6] standard deviation
[7] full width at tenth maximum
[8] line spread function
[9] useful field of view
[10] central field of view
[11] full width at half-maximum

Iv. Discussion

In this study, we developed a gamma detector using large square PMTs which minimizes the required number of PMTs to cover the crystal area. We also reduced 6 × 8 analog signals into a 6 + 8 analog sum of each row and column, enabling reduced analog and digital complexities and improved cost. We converted 14 signals 1 μsec in length to digital using AD9257 high-speed ADCs. The SPARTAN-6 family of FPGA was used to drive ADCs at a rate of 20 million samples per second and to calculate integral values of 14 channels after DC-rejection. Subsequently, the obtained integrations were transmitted to the acquisition computer software for positioning through the UDP Ethernet protocol. The positioning algorithm was based on the digital CSE algorithm which was implemented in the acquisition software.

The performance characteristics of the developed gamma camera were measured using the NEMA NU1 standard. The measured energy resolution in the developed detector was 8.7%, intrinsic spatial resolution was 3.9 mm, uniformity was within 0.6%, and linearity was within 0.1%. We compared the developed detector's parameters with Discovery NM630 GE [25], Infinia GE [26], and Symbia S Siemens [27]. The properties of all detectors are summarized in Table 4. All detectors had similar NaI(Tl) crystal thickness and UFOV area (within 5%). Our detector had 48 square PMTs, while others had a total of 59 PMTs (circular and hexagonal). Using square PMT, our detector showed superior energy resolution, because it left no uncovered area. spatial resolution was in good agreement with the other detectors, in comparison with non-square PMTs. The linearity and the uniformity were superior. The performance evaluation

showed that the developed detector has proper specifications for imaging purposes at a lower cost and with less complexity.

Table 4. Comparison of the developed detector with other similar detectors

Specification	Developed Detector	Discovery NM630 GE [25]	Infinia GE [26]	Symbia S Siemens [27]
Crystal	NaI(Tl)	NaI(Tl)	NaI(Tl)	NaI(Tl)
Thickness (mm)	9.5	9.5	9.5	9.5
PMT shape	Square	Circular	Circular	Hexagonal
PMT size (mm)/pcs	76/48	76/53 38/6	76/53 38/6	76/53 51/6
UFOV (cm^2)	54×38	54×40	54×40	53.3×38.7
Intrinsic Spatial Resolution in CFOV (mm)	≤ 3.9	≤ 3.8	≤ 3.8	≤ 3.8
Intrinsic Energy Resolution (%)	≤ 8.7	≤ 9.5	≤ 9.8	≤ 9.9
Differential Linearity in UFOV (mm)	≤ 0.04	≤ 0.2	≤ 0.1	≤ 0.2
Absolute Linearity in UFOV (mm)	≤ 0.1	≤ 0.5	≤ 0.5	≤ 0.7
Differential Uniformity in UFOV (%)	≤ 0.4	≤ 2.3	≤ 2.3	≤ 2.7
Integral Uniformity in UFOV (%)	≤ 0.6	≤ 3.6	≤ 3.6	≤ 3.7

V. Conclusion

In this study, we introduced novel readout electronics for scintillation detectors using square PMTs. Our approach combined analog and digital signals in positioning reducing 48 signals to 14 signals and improving complexity and cost considerations, while preserving image quality. NEMA NU1 results confirmed that the designed gamma detector had excellent performance and can be used reliably for nuclear medicine imaging.

Declarations

Acknowledgment

This work was supported by Tehran University of Medical Sciences, Grant No. 1401-3-424-63878. The authors would like to appreciate PNP Co. for offering technical support.

References

1. Anger HO. Scintillation camera. Rev Sci Instrum. 1958;29:27–33.
2. Cherry SR, Sorenson JA, Phelps ME, ScienceDirect. (Online service), 2003. Physics in nuclear medicine (Vol. 3).Saunders.
3. Chandra R, Rahmim A. Nuclear medicine physics: the basics. Lippincott Williams & Wilkins; 2017.
4. Peterson TE, Furenlid LR. "SPECT detectors: the Anger Camera and beyond", Physics in medicine and biology, vol. 56, p. R145, 2011.
5. Anger HO. Scintillation camera with multichannel collimators. J Nucl Med. 1964;5:515–31.
6. Boschi A, Uccelli L, Martini P. "A Picture of Modern Tc-99m Radiopharmaceuticals: Production, Chemistry, and Applications in Molecular Imaging", Applied Sciences, vol. 9, p. 2526, 2019.
7. Rassam F, Olthof PB, Bennik RJ, van Guilk TM. “Current Modalities for the Assessment of Future Remnant Liver Function”, Visc Med, vol. 33, pp.442–448, 2017.
8. Park J, Bae S, Seo S, Park S, Bang J-I, Han JH et al. "Measurement of Glomerular Filtration Rate using Quantitative SPECT/CT and Deep-learning-based Kidney Segmentation", Scientific reports, vol. 9, p.4223, 2019.
9. Hutton BF, Erlandsson K, Thielemans K. "Advances in clinical molecular imaging instrumentation", Clinical and Translational Imaging, vol. 6, pp. 31–45, 2018.
10. Cherepy NJ, Payne SA, Asztalos SJ, Hull G, Kuntz JD, Niedermayr T, et al. Scintillators with potential to supersede lanthanum bromide. IEEE Trans Nucl Sci. 2009;56:873–80.
11. Dorenbos P, de Haas JTM, Van Eijk C. Non-proportionality in the scintillation response and the energy resolution obtainable with scintillation crystals. IEEE Trans Nucl Sci. 1995;42:2190–202.
12. Hemmati H, Kamali-Asl A, Haghshenas R. "The Effects of Light Guide Thickness on the Accuracy of Position Estimation, Linearity, and Uniformity Responses of Anger Camera: A Monte Carlo Study", Frontiers in Biomedical Technologies, vol. 2, pp. 172–183, 2015.
13. Wang B, Kreuger R, Beekman FJ, Goorden MC. Novel light-guide-PMT geometries to reduce dead edges of a scintillation camera. Physica Med. 2018;48:84–90.
14. Pani R, Bettiol M, Preziosi E, Cinti M, Borrazzo C, Pellegrini R, et al. Position algorithm for monolithic scintillation crystals based on charge projection readout. J Instrum. 2016;11:C01061.
15. Galasso M, Fabbri A, Borrazzo C, Cencelli VO, Pani R. A Theoretical Model for Fast Evaluation of Position Linearity and Spatial Resolution in Gamma Cameras Based on Monolithic Scintillators. IEEE Trans Nucl Sci. 2016;63:1386–98.
16. Barrett HH, Hunter WC, Miller BW, Moore SK, Chen Y, Furenlid LR. Maximum-likelihood methods for processing signals from gamma-ray detectors. IEEE Trans Nucl Sci. 2009;56:725–35.
17. España S, Deprez K, Van Holen R, Vandenberghe S. Fast calibration of SPECT monolithic scintillation detectors using un-collimated sources. Phys Med Biol. 2013;58:4807.

18. Hung NM, Joung J, Lee K, Kim Y. Development of correction schemes for a small field of view gamma camera. Biomed Eng Lett. 2012;2:215–22.
19. Zeraatkar N, Sajedi S, Fard BT, Kaviani S, Akbarzadeh A, Farahani M, et al. Development and calibration of a new gamma camera detector using large square Photomultiplier Tubes. J Instrum. 2017;12:P09008.
20. Ling T, Lewellen T, Miyaoka R. Depth of interaction decoding of a continuous crystal detector module. Phys Med Biol. 2007;52:2213.
21. Teimourian Fard B, Shamsaei Zafarghandi M. Comparative assessment of the accuracy of maximum likelihood and correlated signal enhancement algorithm positioning methods in gamma camera with large square photomultiplier tubes. Iran J Nuclear Med. 2019;27:81–6.
22. Aliaga R, Martinez J, Gadea R, Sebastia A, Benlloch J, Sánchez F, et al. Corrected position estimation in PET detector modules with multi-anode PMTs using neural networks. IEEE Trans Nucl Sci. 2006;53:776–83.
23. Pierce L, Hunter W, Haynor D, MacDonald L, Kinahan P, Miyaoka R. Multiplexing strategies for monolithic crystal PET detector modules. Phys Med Biol. 2014;59:5347.
24. National Electrical Manufacturers Association, Standards Publication NEMA. NU 1-2018: Performance Measurements of Gamma Cameras. Rosslyn Virginia: National Electrical Manufacturers Association; 2018.
25. GE Healthcare Discovery NM630 Datasheet., 5410645-IEN Rev.1, DOC0963080_Rev 3.0
26. GE Healthcare. Infinia Product data, Release 2.5, Direction 2411980-100 Rev3
27. Siemens Svmbia S. system specification, Order No. A91M1-10128-4T-7600

Figures

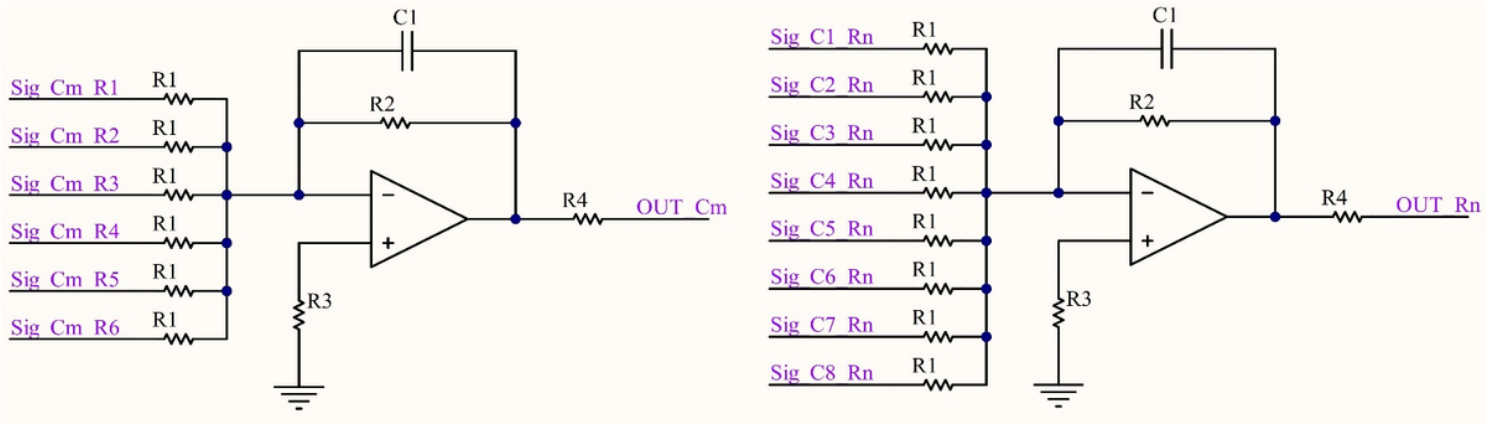

Figure 1

Column (left) and row (right) summation circuits. Each PMT signal (located on C_mR_n) contributes to two summation circuits ($column_m$ and row_n).

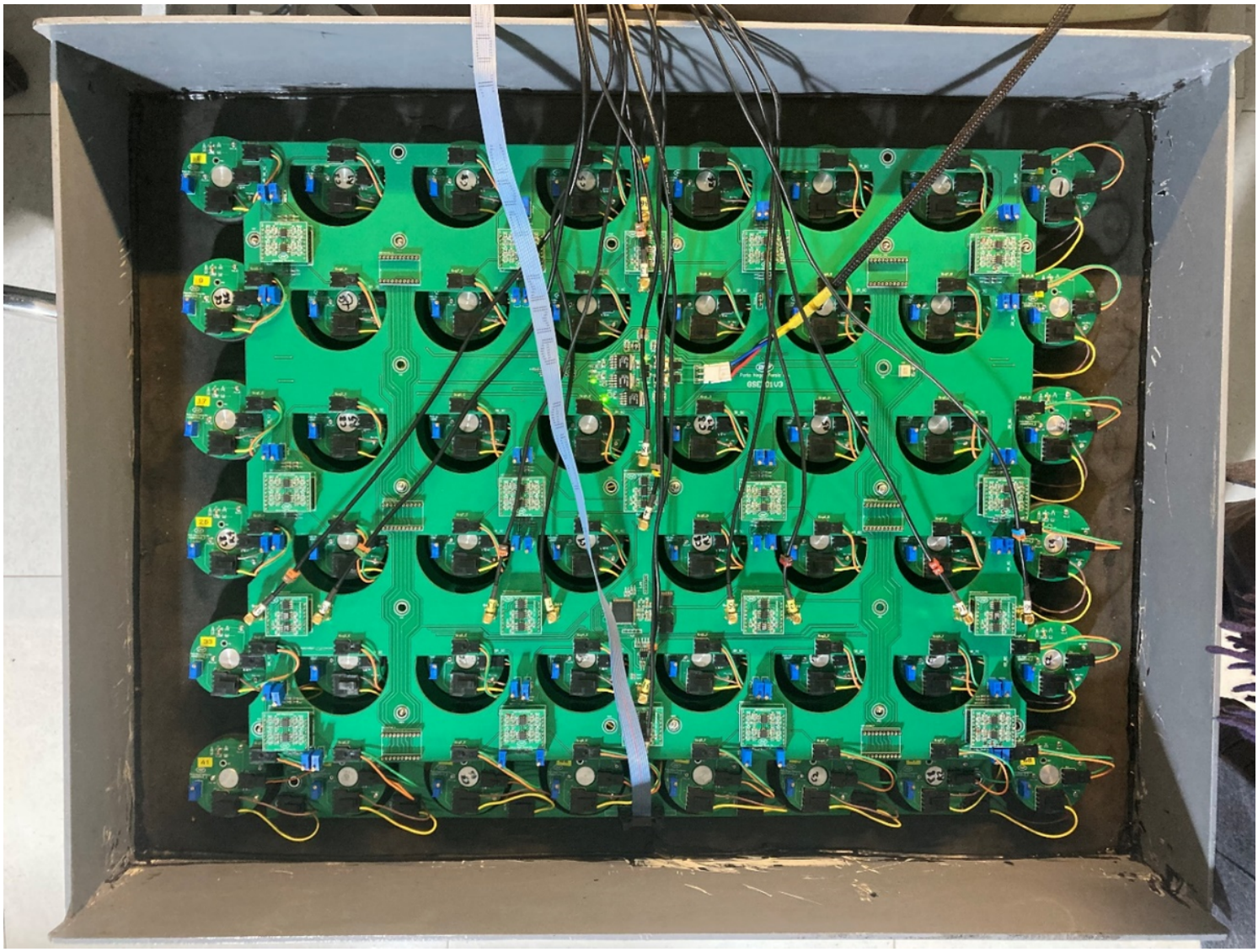

Figure 2

Developed pizza board consisting of preamps and summations circuits. Each preamp is placed close to the corresponding PMT to minimize track length and noise.

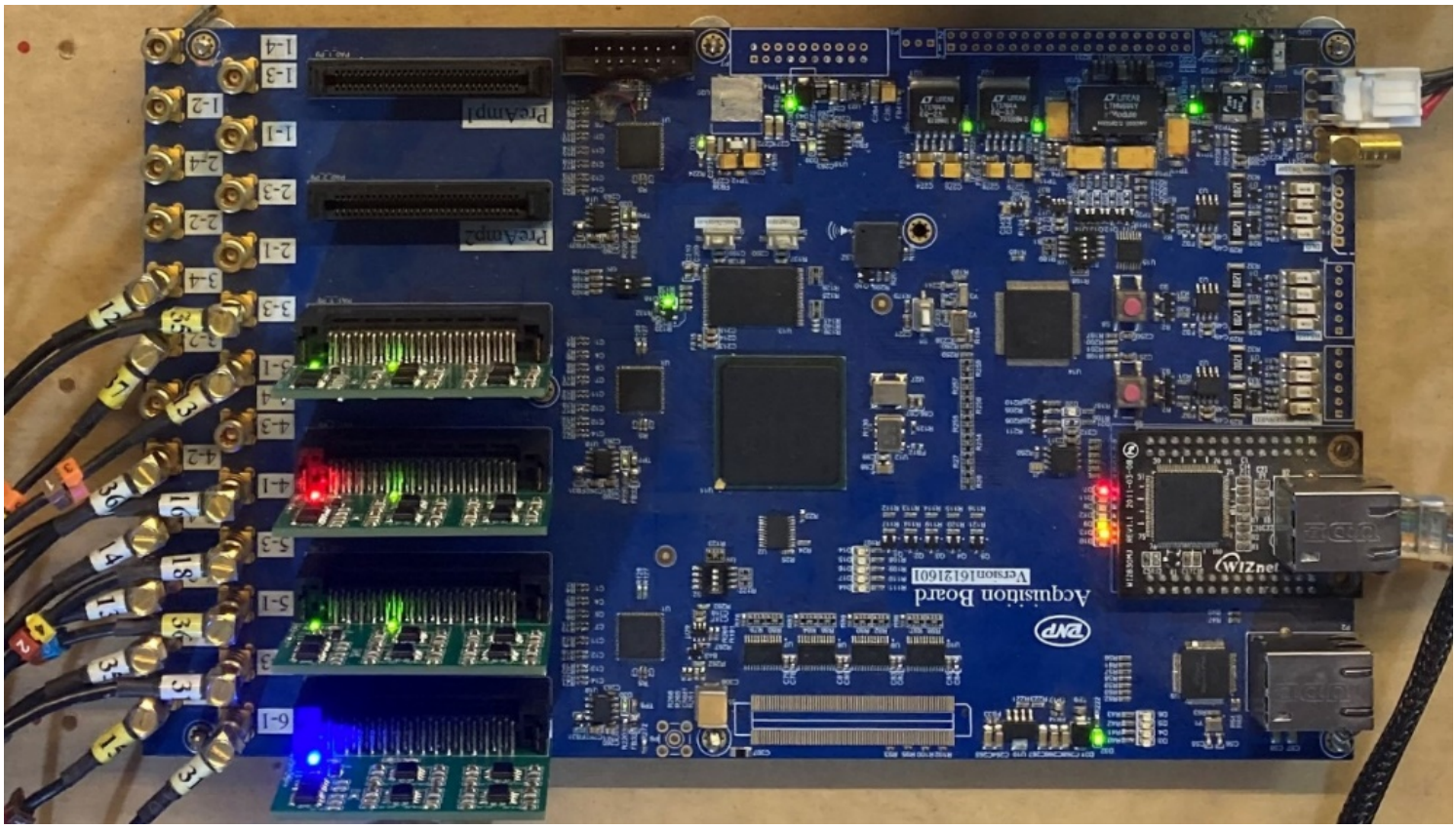

Figure 3

Developed ACQ board consisting of high-speed ADCs, FPGA and WIZnet.

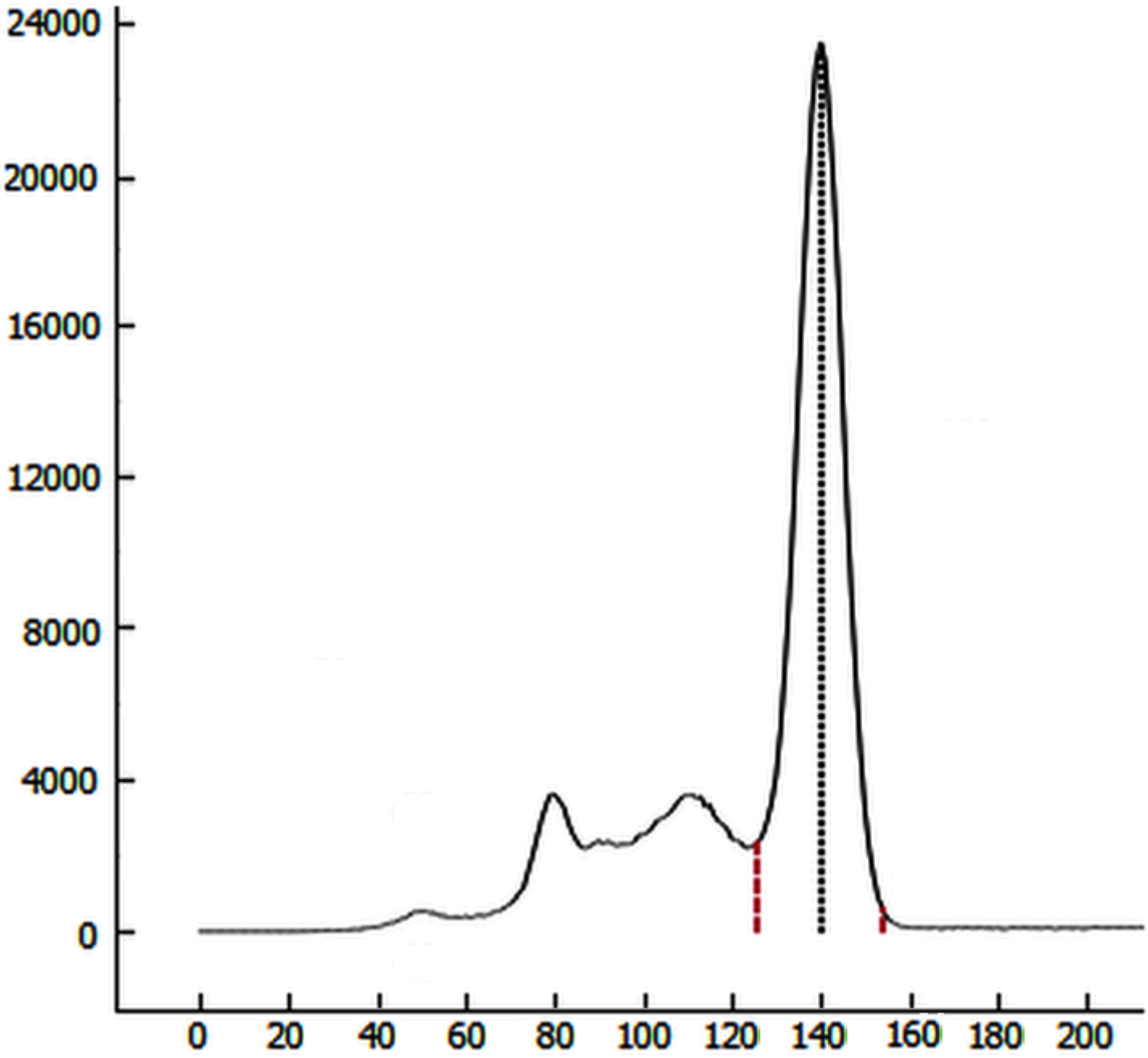

Figure 4

Energy spectrum after energy calibration. Tc-99m 140keV photopeak is clearly visible in the spectrum.

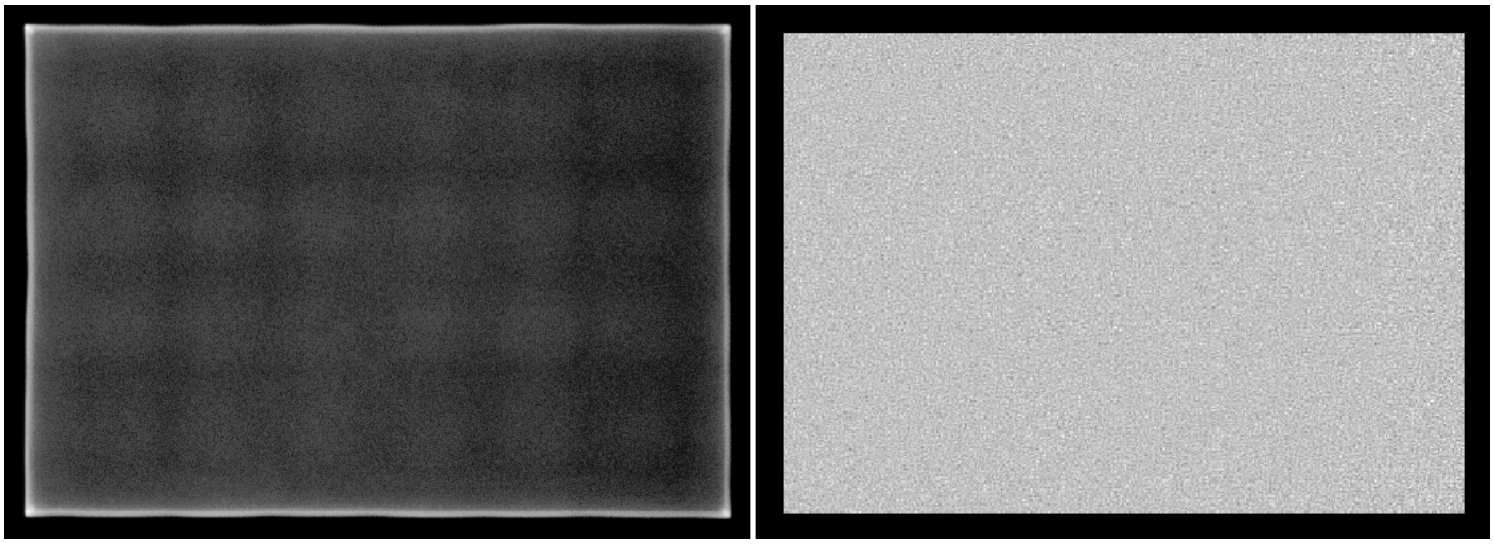

Figure 5

Flood image before (left) and after (right) uniformity calibration. As expected, at the edge area of the detector, the intensity is high duo to lack of positioning data. This area is masked after calibration.

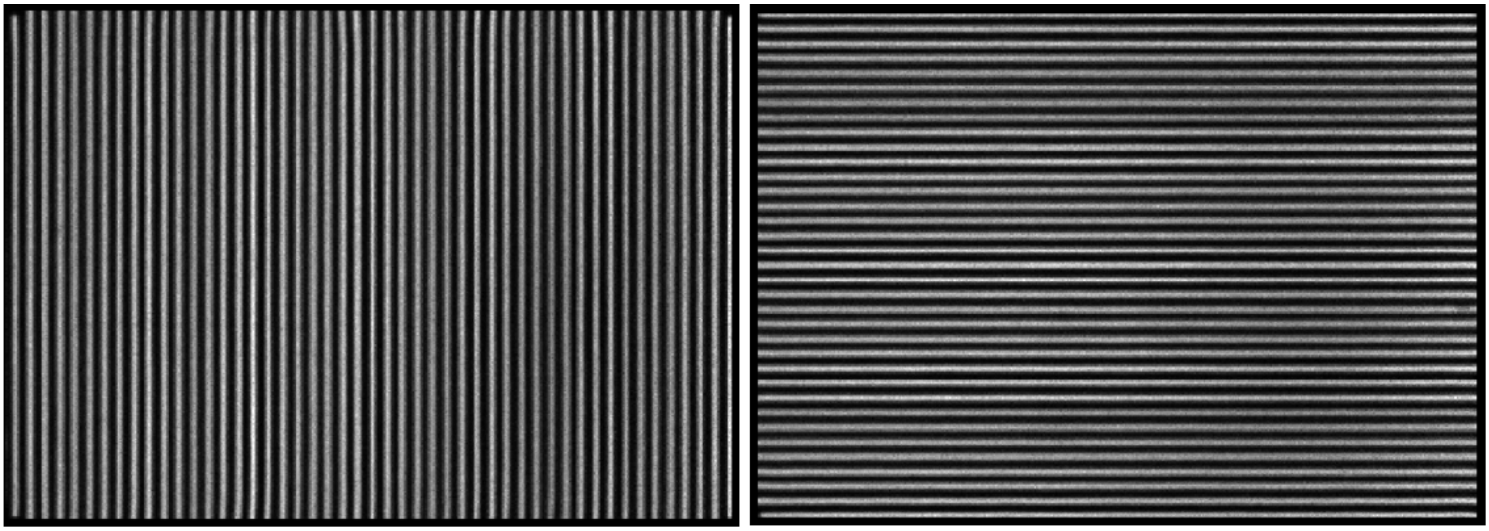

Figure 6

Vertical(left) and horizontal(right) slit mask lead images after calibrations.